EIGENVECTOR BASED BLOCK VECTOR SYNCHRONIZATION WITH APPLICATIONS TO PTYCHOGRAPHIC IMAGING

Nicole Baker[*], *John Flynn*[†], *Jonathan Mousley*[‡], *Yulia Hristova*[§], *Aditya Viswanathan*[§¶]

[*] Oakland University, 146 Library Drive, Rochester, MI 48309
[†] University of California San Diego, 9500 Gilman Drive, La Jolla, CA 92093
[‡] Duke University, 120 Science Drive, 117 Physics Building, Box 90320, Durham, NC 27708
[§] University of Michigan – Dearborn, 4901 Evergreen Road, Dearborn, MI 48128

ABSTRACT

We consider the problem of recovering a complex vector (up to a global unimodular constant) given noisy and incomplete outer product measurements. Such problems arise when implementing distributed clock synchronization schemes, radar autofocus methods, and phaseless signal recovery. This problem is known as *vector synchronization* and is a variant of the more common *angular synchronization* problem. In applications with windowed measurements and/or convolutional models - for example, phase retrieval from STFT magnitude data, the outer product measurement matrix is highly incomplete and has a block diagonal structure. We describe a vector synchronization technique which applies an eigenvector computation to blocks of this matrix followed by a block compatibility operation to piece together the final solution. We provide theoretical guarantees (in the noiseless case) and empirical simulations demonstrating the accuracy and efficiency of the method.

Index Terms— Vector Synchronization, Phaseless Imaging, Magnitude-only STFT Inversion

1. INTRODUCTION

We consider the problem of recovering (up to a global phase constant) a complex vector $\mathbf{x} = \begin{bmatrix} x_0 & x_1 & \dots & x_{n-1} \end{bmatrix}^T \in \mathbb{C}^n$, $n \in \mathbb{N}$ given the "measurement" matrix $Z \in \mathbb{C}^{n\times n}$ with

$$Z_{jk} = \begin{cases} x_j\overline{x}_k + \eta_{jk}, & (j,k) \in E, \\ 0, & (j,k) \notin E. \end{cases} \tag{1}$$

Here $\eta_{jk} \sim \mathbb{C}\mathcal{N}(0,\sigma^2)$ denotes independent and identically distributed (circularly symmetric) complex Gaussian noise with variance σ^2, $\overline{a}$ is the complex conjugate of $a \in \mathbb{C}$ and $E \subseteq \{0,1,\dots,n-1\}^2$ denotes an index set containing the (ordered pair) entries for which measurements are available. This problem is known as *vector synchronization* and is a variant of the more common *angular synchronization* problem [1] where we recover n distinct angles $\{\theta_i\}_{i=0}^{n-1}$ given angular differences or *offsets*. Indeed, if $\mathbf{x}$ is unimodular ($|x_j| = |e^{i\theta_j}| = 1,\ j = 0,\dots,n-1$), we obtain the angular synchronization problem. Such problems arise in clock synchronization schemes in distributed network settings [2], certain imaging modalities (such as structured lifting techniques for phaseless image recovery) [3] and when correcting for systemic (autofocus) errors in radar imaging [4].

With perfect and complete measurements (i.e., $\eta_{jk} = 0$ and $E = \{0,1,\dots,n-1\}^2$), we have $Z = \mathbf{x}\mathbf{x}^*$ (with $\mathbf{x}^*$ denoting the conjugate transpose of $\mathbf{x}$). Hence, we may recover $\mathbf{x}$ by computing the (scaled) leading eigenvector (corresponding to the largest eigenvalue) of the rank-1 matrix Z. We are, however, interested in recovering $\mathbf{x}$ when Z has structure as follows:

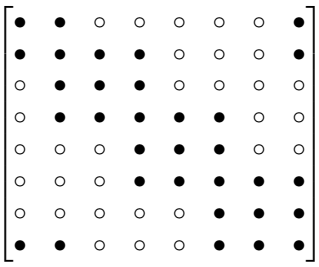

with the •s denoting entries included in the index set E. Such index sets arise in problems with convolutional models and/or windowed measurements such as *ptychographic* phaseless imaging [5], which can be cast as a problem of signal recovery from STFT magnitude measurements.

A simple eigenvector computation as in the case with perfect and complete measurements no longer works. An equivalent procedure (after entrywise normalization of the nonzero entries) may still be used to recover $\mathbf{x}$; however, there are a few important caveats. To start with, the corresponding Z is no longer rank-1. It is also possible to show (see [3]) that the

This research was completed at the REU Site: Mathematical Analysis and Applications at the University of Michigan–Dearborn. We thank the National Science Foundation (DMS-2012238), the College of Arts, Sciences, and Letters (CASL), and the Department of Mathematics and Statistics for their support.

¶ This author was supported in part by the Air Force Office of Scientific Research (FA9550-22-1-0411).

spectral gap reduces as the block size reduces or the problem size increases. This can lead to reduced accuracy and robustness when using traditional vector synchronization methods.

Related Work and Contributions

The more common angular synchronization problem has been addressed previously (see, for example, [1]) via methods such as eigenvector, graph-based, and semi-definite programming methods. We propose an eigenvector technique which is motivated by the methods described in [1] and [3] and applies to the above practically important block structured measurement setting. A similar procedure was utilized in [6] to improve the *magnitude* recovery in ptychographic reconstruction schemes. Additionally, the dissertation [7] contains graph-theoretic analysis of the angular and vector synchronization problems, including a theoretical robustness bound for the setting discussed in this paper. It is remarked in [7], however, that this bound is overly pessimistic. Numerical results in this paper confirm this conjecture by showing that the proposed method provides excellent robustness and computational efficiency, and is even amenable to parallel computations.

The rest of this paper is organized as follows: §2 summarizes the connection between vector synchronization and phaseless ptychographic imaging, while §3 discusses the block vector synchronization method. Numerical experiments confirming the efficacy and robustness of the method are provided in §4, while §5 provides some concluding remarks.

2. PTYCHOGRAPHIC IMAGING

Ptychography [5] is a diffractive imaging technique where overlapping *local* regions of a specimen under study are illuminated by electromagnetic radiation of appropriate wavelength in a raster scan fashion. Diffraction pattern measurements corresponding to each of these illuminations are then combined together computationally to recover the specimen. The physics of the imaging process means that the diffraction patterns are (squared) magnitude-only measurements; nevertheless, by incorporating a suitable window or mask between the radiation source and specimen, phase relationships between the components of the specimen can be encoded in the phaseless measurements. All that remains is to solve a phase retrieval problem [8, 9] to recover the phase and the specimen.

A discrete, 1D abstraction of this problem can be written as follows: find (up to multiplications with a single unimodular constant) $\mathbf{x} \in \mathbb{C}^n$ given the phaseless measurements

$$(\mathbf{y}_\ell)_j = \left|\left\langle \mathbf{x}, S_\ell^* \mathbf{m}^{(j)} \right\rangle\right|^2, \quad (\ell, j) \in \{0, 1, \ldots, n-1\}^2, \tag{2}$$

where $S_\ell : \mathbb{C}^n \to \mathbb{C}^n$, $(S_\ell \mathbf{x})_j := x_{j+\ell}$ is a circular shift operator (with all indexing considered modulo-n), and $\{\mathbf{m}^{(j)}\}$ are a set of *local* masks with each $\mathbf{m}^{(j)} \in \mathbb{C}^n$ having nonzero entries in only the first $s \in \mathbb{N}\ (< n/2)$ indices. The shift operator models the raster scan process in ptychography while the support constraint on $\mathbf{m}^{(j)}$ models the local illumination. The measurement $(\mathbf{y}_\ell)_j$ hence corresponds to a shift index ℓ and and mask index j. Depending on the imaging setup, fewer than the full set of n shifts and/or n masks are typically used. Note that (2) is nonlinear (and indeed, highly non-convex) in the variable $\mathbf{x}$, making convergent solutions difficult to compute and guarantee. However, using a lifting argument [10], we may linearize the measurements (denoted by $\mathcal{A}$ below) in terms of the rank-1 matrix variable $\mathbf{x}\mathbf{x}^*$, with

$$(\mathbf{y}_\ell)_j = \left|\left\langle \mathbf{x}, S_\ell^* \mathbf{m}^{(j)} \right\rangle\right|^2 = \underbrace{\left\langle \mathbf{x}\mathbf{x}^*, S_\ell^* \mathbf{m}^{(j)} \mathbf{m}^{(j)^*} S_\ell \right\rangle_{\text{HS}}}_{\mathcal{A}(\mathbf{x}\mathbf{x}^*)_{\ell,j}} \tag{3}$$

where $\langle \cdot, \cdot \rangle : \mathbb{C}^n \times \mathbb{C}^n \to \mathbb{C}$, $\langle A, B \rangle_{\text{HS}} = \text{trace}(AB^*)$ is the Hilbert-Schmidt inner product. Furthermore, due to the local support constraints on the masks – characterized by the parameter s – and the set of shifts $\{\ell\}$, the measurements only depend on a *subset* of entries of $\mathbf{x}\mathbf{x}^*$. In particular,

$$(\mathbf{y}_\ell)_j = \left\langle T_s(\mathbf{x}\mathbf{x}^*), S_\ell^* \mathbf{m}^{(j)} \mathbf{m}^{(j)^*} S_\ell \right\rangle_{\text{HS}}$$

where $T_s : \mathbb{C}^{n \times n} \to \mathbb{C}^{n \times n}$ is a matrix restriction defined as

$$\left(T_s(A)\right)_{jk} = \begin{cases} A_{jk}, & (j,k) \in E \\ 0, & (j,k) \notin E \end{cases}$$

with E being an index set as in (1). For well designed measurements, we have $\text{Span}\{S_\ell^* \mathbf{m}^{(j)} \mathbf{m}^{(j)^*} S_\ell\}_{\ell,j} = T_s\left(\mathbb{C}^{n \times n}\right)$, and inverting the *linear* system $\mathcal{A}|_{T_s(\mathbb{C}^{n\times n})}$ yields $T_s(\mathbf{x}\mathbf{x}^*)$. This leads us to the vector synchronization problem introduced in §1 since $T_s(\mathbf{x}\mathbf{x}^*) = Z$ in the case of perfect (noiseless and invertible) measurements.

3. BLOCK VECTOR SYNCHRONIZATION

By definition of (1) and the block structure of Z, we note that each block is locally rank-1. Hence, we may compute the

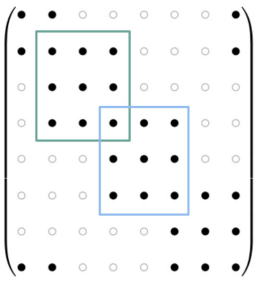

Fig. 1: Illustrating block eigenvector computations

leading eigenvectors of the individual blocks accurately (due to the rank-1 structure), efficiently (due to the typically small

block size) and (if needed) in parallel. For the example in Fig. 1, the eigenvectors corresponding to the two indicated blocks are denoted as $\mathbf{u}^{(1)}$ (corresponding to the green block) and $\mathbf{u}^{(2)}$ (corresponding to the blue block), where we have

$$\mathbf{u}^{(1)} = c_1 \begin{bmatrix} \widehat{x}_1 & \widehat{x}_2 & \widehat{x}_3 \end{bmatrix}^T, \quad \mathbf{u}^{(2)} = c_2 \begin{bmatrix} \widehat{x}_3 & \widehat{x}_4 & \widehat{x}_5 \end{bmatrix}^T.$$

Here $\widehat{x}_j$ denotes an approximation to the true component x_j. Since any multiple of an eigenvector is also an eigenvector, $c_1, c_2 \in \mathbb{C}$ denote unavoidable local scale factors. The overlap of the blocks in Fig. 1, however, means that the last entry of $\mathbf{u}^{(1)}$ and the first entry of $\mathbf{u}^{(2)}$ should coincide. More generally (as shown in Fig. 2), we require the last $s-\alpha$ entries of block $\mathbf{u}^{(\ell-1)}$ coincide with the first $s-\alpha$ entries of block $\mathbf{u}^{(\ell)}$ where $s, \alpha \in \mathbb{N}$ (with $s > \alpha$) and s denotes the block size. These subvectors are denoted (and shaded red) as $\widetilde{\mathbf{u}}^{(\ell-1)}$ and $\widetilde{\mathbf{u}}^{(\ell)}$ respectively in Fig. 2. To resolve incompatibilities in magnitude between the blocks, we set

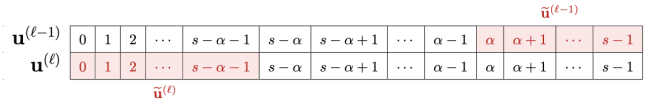

Fig. 2: Illustrating block compatibility operations

$$\mathbf{u}^{(\ell)} \leftarrow \frac{\|\widetilde{\mathbf{u}}^{(\ell-1)}\|_2}{\|\widetilde{\mathbf{u}}^{(\ell)}\|_2} \mathbf{u}^{(\ell)} \tag{4}$$

while incompatibilities in the phase are resolved by setting

$$\mathbf{u}^{(\ell)} \leftarrow \omega \mathbf{u}^{(\ell)}, \quad \omega = \frac{\langle \widetilde{\mathbf{u}}^{(\ell-1)}, \widetilde{\mathbf{u}}^{(\ell)} \rangle}{\langle \widetilde{\mathbf{u}}^{(\ell-1)}, \widetilde{\mathbf{u}}^{(\ell-1)} \rangle} \tag{5}$$

where $\langle \mathbf{x}, \mathbf{y} \rangle = \mathbf{y}^* \mathbf{x}$ denotes the complex inner product. These block compatibility operations ensure that the overlapping portions of the vectors agree with each other (i.e., they are synchronized). Applying these to all pairs of successive blocks (and noting the use of circular indexing), we obtain Alg. 1. For ease of exposition, we have utilized the maps $R_1, R_2 : \mathbb{C}^s \to \mathbb{C}^{s-\alpha}$ which extract the last and first $s-\alpha$ entries respectively given a vector $\mathbf{u} \in \mathbb{C}^s$, where

$$R_1 \left(\begin{bmatrix} u_0 \\ u_1 \\ \vdots \\ u_{s-1} \end{bmatrix} \right) = \begin{bmatrix} u_\alpha \\ u_{\alpha+1} \\ \vdots \\ u_{s-1} \end{bmatrix}, \; R_2 \left(\begin{bmatrix} u_0 \\ u_1 \\ \vdots \\ u_{s-1} \end{bmatrix} \right) = \begin{bmatrix} u_0 \\ u_1 \\ \vdots \\ u_{s-\alpha-1} \end{bmatrix}.$$

Similarly, we denote by $Z^{(\ell-1)}$ and $Z^{(\ell)}$ successive rank-1 blocks of Z (see highlighted boxes in Fig. 1 for illustration). We note that any of the blocks may be denoted $Z^{(0)}$ for initialization purposes. A block $Z^{(\ell)}$ typically consists of the s^2 entries $Z_{p_\ell:p_\ell+s-1, p_\ell:p_\ell+s-1}$ for a suitable $p_\ell \in \mathbb{Z}_n$ with all indexing[1] considered modulo-n. The succeeding block will then contain the entries $Z_{p_\ell+\alpha:p_\ell+\alpha+s-1, p_\ell+\alpha:p_\ell+\alpha+s-1}$.

[1] we use Matlab indexing notation here for simplicity

Algorithm 1 Eigenvector-based block vector synchronization

Input: Measurements $Z \in \mathbb{C}^{n \times n}$ as per (1); block size s; overlap parameter α

Output: Estimate $\widehat{\mathbf{x}} \in \mathbb{C}^n$ of the unknown signal $\mathbf{x}$

1: Set $Z \leftarrow (Z + Z^*)/2$ to enforce Hermitian symmetry.
2: Compute $\lambda^{(0)}$ and $\mathbf{u}^{(0)}$ – the largest (in magnitude) eigenvalue and corresponding eigenvector of $Z^{(0)}$ and set $\widehat{x}_k = \sqrt{\lambda^{(0)}}\, u_k^{(0)}$, $k = p_0, \ldots, p_0 + s - 1$.
3: **for** $\ell = 1, \ldots, \frac{N}{\alpha} - 1$ **do**
4: Compute eigenpair $\lambda^{(\ell)}$, $\mathbf{u}^{(\ell)}$ corresponding to $Z^{(\ell)}$
5: Extract overlapping entries in the successive blocks

$$\widetilde{\mathbf{u}}^{(\ell-1)} = R_1 \mathbf{u}^{(\ell-1)}, \quad \widetilde{\mathbf{u}}^{(\ell)} = R_2 \mathbf{u}^{(\ell)}$$

6: Apply block compatibility operations (4) and then (5)
7: Update output estimate

$$\widehat{x}_k = u_k^{(\ell)}, \quad k = p_\ell, \ldots, p_\ell + s - 1.$$

8: **end for**

By using the power method for eigenvector computations, we can show that the method is essentially linear time with cost $\mathcal{O}\left(ns^2/\alpha\right)$. Moreover, we have the following theoretical result in the noiseless (perfect measurements) setting.

Lemma 1. *Let $Z \in \mathbb{C}^{n \times n}$ be an admissible measurement matrix as defined in* (1) *with η_{jk} identically zero for all $(j,k) \in \{0, 1, \ldots, n-1\}^2$. Alg. 1 computes an estimate $\widehat{\mathbf{x}}$ of the true signal $\mathbf{x} \in \mathbb{C}^n$ such that $\widehat{\mathbf{x}} = \omega \mathbf{x}$ where $\omega \in \mathbb{C}$ is a unimodular ($|\omega| = 1$) constant.*

Proof. The proof follows from the definition of Z, the rank-1 property of each of the blocks $Z^{(\ell)}$, and noting that the block compatibility operations (4) and (5) yield perfect synchronization in the case of noiseless measurements. □

4. NUMERICAL RESULTS

We now provide representative results from empirical simulations. Results in this section were obtained using a laptop computer (Apple MacBook Pro with 16GB RAM and Intel Core i5 quad-core processor) in Matlab (R2021a). Data points in the figures were obtained by averaging results from 50 trials. For noise robustness experiments, we report the added noise level (as well as reconstruction errors) in the form of signal to noise ratios (SNR) in decibels (dB), with

$$\text{SNR (dB)} = 10 \log_{10} \left(\frac{\|X\|_F^2}{\|Z - X\|_F^2} \right)$$

$$\text{Error (dB)} = 10 \log_{10} \left(\frac{\min_{|\omega|=1} \|\omega \, \widehat{\mathbf{x}} - \mathbf{x}\|_2^2}{\|\mathbf{x}\|_2^2} \right)$$

where X, $\mathbf{x}$ and $\widehat{\mathbf{x}}$ denote the noise-free measurement matrix, true signal and estimate returned by Alg. 1 respectively.

Fig. 3 plots the recovery error (in dB) versus the noise level (SNR, in dB) when using Alg. 1. The problem and block sizes are fixed to be $n = 150$ and $s = 11$ respectively. Plots for various overlap parameters α are shown in Fig. 3. Note that the noise level decreases (with increasing SNR) as we move from left to right in the figure. As observed, we expect to see straight line plots with roughly unit negative slope and suitable vertical offset; this indicates recovery up to the level of added noise. We also see that larger overlaps (smaller α values) provide better robustness – in these cases, more entries are used in block compatibility operations.

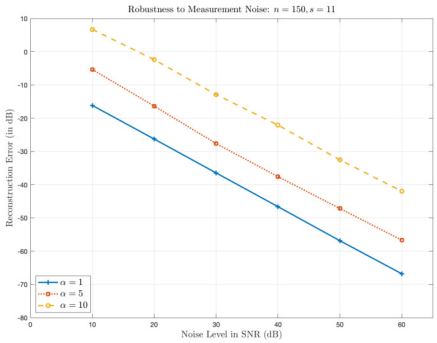

Fig. 3: Noise robustness of the proposed method

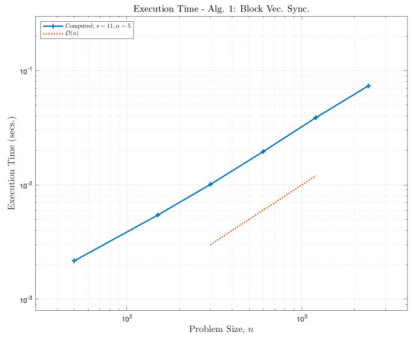

(a) Computational cost as a function of problem size n

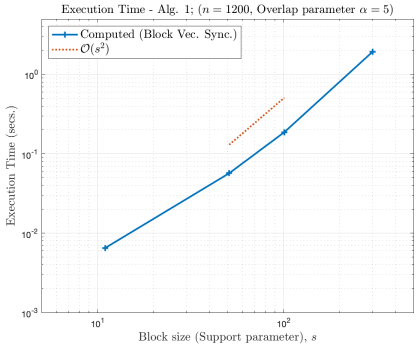

(b) Computational cost as a function of block size s

Fig. 4: Computational efficiency simulations for Alg. 1

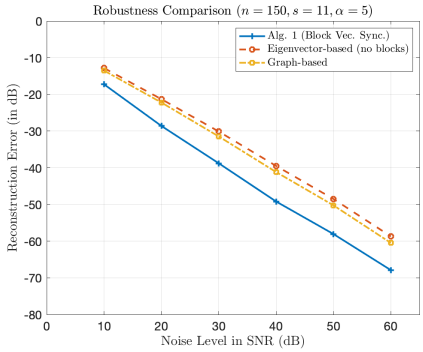

(a) Comparing the noise robustness of Alg. 1 with other methods

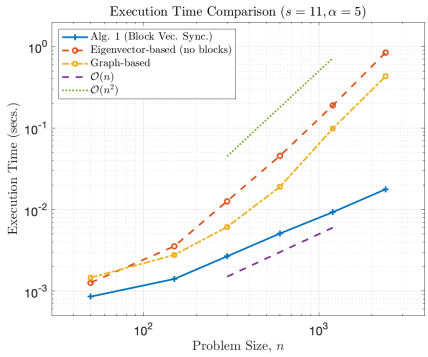

(b) Comparing the computational cost of Alg. 1 with other methods

Fig. 5: Comparisons with other methods

We next provide results confirming the computational cost and efficiency of Alg. 1. Fig. 4a plots the execution time for implementing Alg. 1 as a function of the problem size n. We see that the execution time scales linearly as predicted in §3. Similarly, Fig. 4b plots the the execution time for various block sizes s. Here, the execution time scales as $\mathcal{O}(s^2)$; once again, this agrees with the prediction in §3. Finally, Fig. 5 compares the performance of the proposed technique with other methods from literature, including one based on spectral analysis of a weighted graph Laplacian [7] and a classical (non-block based) eigenvector method [1]. These plots confirm that Alg. 1 is a computationally efficient and robust method for performing vector synchronization.

5. CONCLUSION

In this paper, we discussed a block eigenvector-based technique for the vector synchronization problem. Empirical results confirm the accuracy, robustness and computational efficiency of the method. Possible avenues for future research include statistical estimation-theoretic analysis of the method, deriving improved robust recovery guarantees (for example, improving on the results from [7]), incorporation into existing phaseless imaging algorithms, and considering constrained or relaxed variants of the problem.

6. REFERENCES

[1] A. Singer, "Angular synchronization by eigenvectors and semidefinite programming," *App. Comp. Harmonic Anal.*, vol. 30, no. 1, pp. 20–36, Jan. 2011.

[2] A. Giridhar and P. R. Kumar, "Distributed clock synchronization over wireless networks: Algorithms and analysis," in *Proc. 45th IEEE Conf. Decision and Control*, Dec. 2006, pp. 4915–4920.

[3] A. Viswanathan and M. Iwen, "Fast angular synchronization for phase retrieval via incomplete information," in *Proc. Wavelets and Sparsity XVI*. Aug. 2015, vol. 9597, pp. 281–288, SPIE.

[4] T. Scarnati and A. Gelb, "Joint image formation and two-dimensional autofocusing for synthetic aperture radar data," *J. Comp. Phy.*, vol. 374, pp. 803–821, Dec. 2018.

[5] J. M. Rodenburg, "Ptychography and related diffractive imaging methods," in *Adv. Imag. and Electron Phy.*, Hawkes, Ed., vol. 150, pp. 87–184. Elsevier, Jan. 2008.

[6] B. Preskitt and R. Saab, "Admissible measurements and robust algorithms for ptychography," *J. Fourier Anal. Appl.*, vol. 27, no. 2, pp. 8, Feb. 2021.

[7] B. P. Preskitt, *Phase Retrieval from Locally Supported Measurements*, Ph.D. thesis, University of California, San Diego, 2018.

[8] Y. Shechtman, Y. C. Eldar, O. Cohen, H. N. Chapman, J. Miao, and M. Segev, "Phase retrieval with application to optical imaging: A contemporary overview," *IEEE Signal Process. Mag.*, vol. 32, no. 3, pp. 87–109, May 2015.

[9] J. Dong, L. Valzania, A. Maillard, T. Pham, S. Gigan, and M. Unser, "Phase retrieval: From computational imaging to machine learning: A tutorial," *IEEE Signal Process. Mag.*, vol. 40, no. 1, pp. 45–57, Jan. 2023.

[10] E. J. Candès, T. Strohmer, and V. Voroninski, "PhaseLift: Exact and stable signal recovery from magnitude measurements via convex programming," *Commun. Pure Appl. Math.*, vol. 66, no. 8, pp. 1241–1274, 2013.